〈Technical Note〉

EXPERIMENTAL APPROACHES FOR WATER DISCHARGE CHARACTERISTICS IN PEMFC USING NEUTRON IMAGING TECHNIQUE AT CONRAD, HMI

TAEJOO KIM[1,2], JONGROK KIM[1], CHEULMUU SIM[2], SUNGHO LEE[3], YOUNGJIN SON[3] and MOOHWAN KIM[1*]
[1]Dept. of Mechanical Engineering, Pohang University of Science and Technology
San 31, Hyoja-dong, Namgu, Pohang, Kyoungbuk, 790-784, Korea
[2]Korea Atomic Energy Research Institute
150 Deokjin-dong, Yuseong-gu, Daejeon, 305-353, Korea
[3]Research & Development Division for Hyundai Motor Company & Kia Motors Corporation
104, Mabuk-Dong, Giheung-Gu, Yongin-Si,Gyunggi-Do, 446-912, Korea
*Corresponding author. E-mail : mhkim@postech.ac.kr

Received April 3, 2008
Accepted for Publication September 8, 2008

In this investigation, we prepared a 1 and 3-parallel serpentine single PEMFC, which has an active area of 100 cm^2 and a flow channel cross section of 1x1mm. Distribution and transport of water in a non-operating PEMFC were observed by varying flow types and the flow rates (250, 400, and 850 cc/min). This investigation was performed at the neutron imaging facility at the COld Neutron RAdiography facility (CONRAD), HMI, Germany of which the collimation ratio and neutron fluence rate are 250, 1×10^6 n/s/cm^2, respectively. The neutron image was continuously recorded by a scintillator and lens-CCD coupled detector system every 10 seconds. It has been observed that although the distilled water was supplied into the cathode channel only, the neutron image showed a water movement from the cathode to the anode channel. The water at the cathode channel was completely discharged as soon as the pressurized air was supplied. But the water at the anode channel was not easily removed by the pressurized air except for the 3-parallel serpentine type with 850 cc/min of air flow rate. Moreover, the water at the MEA wasn't removed for any of the cases.

KEYWORDS : Neutron Imaging Technique; PEMFC; Visualization; Water Management

1. INTRODUCTION

Since the Polymer Electrolyte Membrane Fuel Cell (PEMFC) offers the possibility of low emission and high efficiency power for vehicular applications, it has recently become one of the main research areas for such applications. PEMFC usually uses hydrogen and oxygen as fuel in order to produce electricity. Water, which is one of the byproducts, causes serious problems since the proton conductivity of the membrane is highly influenced by the water content. If the water content at the MEA and channel is too low, the conductivity of the proton is decreased and the efficiency is reduced. Conversely, too much water content causes a flooding at the channel. This flooding impedes gas flow and also reduces the efficiency. Therefore, it is necessary to visualize the channel and MEA of the PEMFC to properly maintain water content and distribution [1].

There have been many research projects [2-12] that have looked at developing measurement methods that will aid in assessing all aspects of a fuel cell operation. However, ascertaining where water is accumulated within a fuel cell, and how it is transported on anode and cathode sides, remains a difficult experimental problem. Recently, new novel experimental designs have been reported that enable a visualization of two-phase flow in cathode flow field channels of PEMFC. For example, Tuber et al. [13] have used a fuel cell with windows to afford visual access. However, this approach limits visualization to the process of water droplets passing from the diffusion medium into the flow field channels. Moreover, this method affects the thermal characteristics of the PEMFC during modification. Perhaps the neutron imaging technique is the only method available for measuring water distribution within an operating fuel cell. Because of the high neutron attenuation of hydrogen relative to other materials used in fuel cell construction, this technique is ideally suited as a way to interrogate an operating fuel cell for water. Several research organizations have developed a high level of expertise in this field.

These organizations have reported experimental work on the application of neutron imaging techniques to fuel cells.

Since an auto-vehicle, which is a main user of PEMFC, can run in sub-zero temperature conditions, the freezing of water at the MEA and channel causes damage to the MEA. Therefore, water at the PEMFC, regardless of its position, must be removed as soon as possible. However, until now there has been little research into the idea of water removal at the PEMFC under various conditions except for our previous research [12]. We used thermal neutron in order to investigate the water behavior in PEMFC in that previous work. However, the characteristics of cold neutrons are different from those of thermal neutrons, and especially it is known that the water attenuation coefficient of cold neutrons is higher than that of thermal neutrons. This means that cold neutrons are more sensitive for investigating water distribution and behavior in PEMFC than thermal neutrons. The research projects that have used cold neutrons for PEMFC are also few and far between. So, for the present study, the water discharge characteristics were investigated by using a neutron imaging technique, especially cold neutrons, and a feasibility test apparatus.

2. EXPERIMENTAL SETUP AND NEUTRON IMAGING TECHNIQUE SYSTEM

2.1 Experimental Setup

In order to investigate water discharge characteristics at PEMFC, the feasibility test apparatus was set up at the COld Neutron RAdiography facility (CONRAD), HMI. Although the objective of the present study was to investigate the water removal characteristics at an operating PEMFC, we couldn't use the actual test station due to the problem of the explosiveness of hydrogen. However, the actual situation could be simulated by using a feasibility test apparatus. The feasibility test apparatus consisted of two parts: one is a distilled water supply loop and the other is a pressurized air loop as shown in Figure 1.

Because the water generated during the operation of the PEMFC usually exists at the cathode side, the distilled water is supplied into the cathode side only by using pressurized air and a water tank system. Since the PEMFC is opaque, it is difficult to know how much water exists in the cathode channel. So, the water is supplied for about ten minutes into the cathode channel. The valve located at the outlet of the PEMFC is closed in order to entrap the water in the cathode channel while supplying pressurized air. When the pressurized air isn't supplied to cathode side, the valve at the outlet of the PEMFC is opened. Finally the neutron images are taken with different flow field types and flow rates. When one test condition is over, we supplied pressurized air into the cathode and anode side in order to remove water from the fuel cell. Table 1 shows the experimental conditions for the investigation of the water removal efficiency.

The two geometries sketched in Figure 2 were chosen to investigate the water discharge characteristics with an active area of 100 cm^2/single-cells. One illustration is a 1-parallel serpentine and the other is a 3-parallel serpentine type. The flow fields were directly machined into a carbon-graphite block. Both types have the same channel width and depth of 1 mm, and the width of rib is 0.5 mm.

Table 1. Experimental Conditions

Flow Field Type	Flow Rate [cc/m]	Fuel Cell Temperature [°C]
1& 3-parallel serpentine	200, 400, 850	30

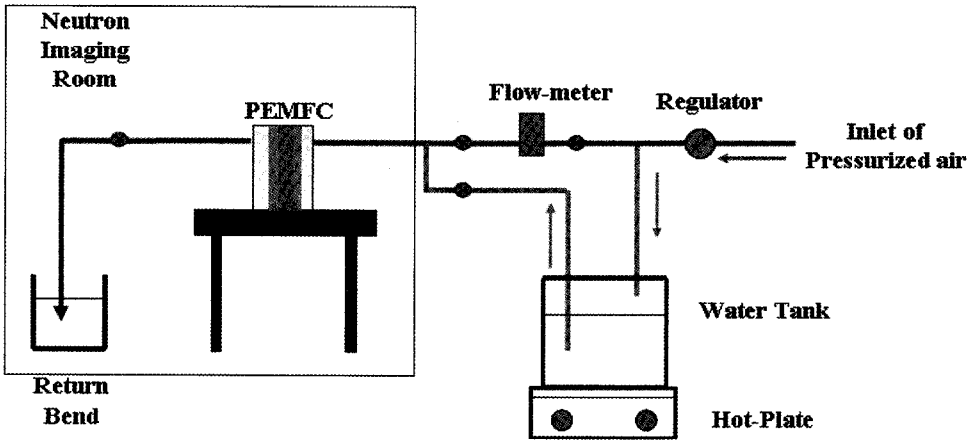

Fig. 1. Schematic Diagram of Test Apparatus

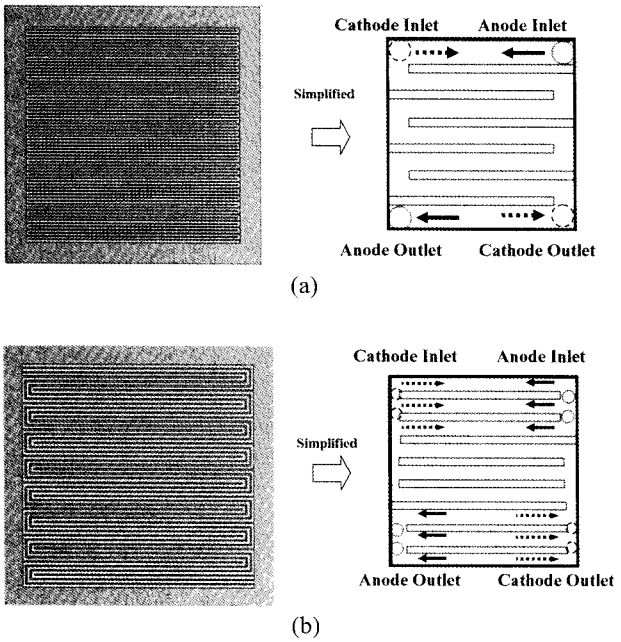

Fig. 2. Schematic Diagram of the Investigated Flow Field Geometries: a) Shows a Continuous Flow Field with a 1-Parallel Serpentine, b) Shows a Continuous Flow Field with a 3-Parallel Serpentine

Although the flow fields used for the anode and cathode are symmetric, the flow direction is opposite. Since the flow direction is opposite, we can easily discriminate the water position in the movie made from the neutron images. We used Nafion-112 for the membrane and platinum of 1 mg/cm^2 was loaded on the cathode and anode, respectively. Two 200μm carbon papers, serving as gas diffusion layers (GDL), were added onto the MEA.

Before and after discharging testing, polarization curves were drawn in order to check the level of damage of the PEMFC. Since we didn't have an actual test station at HANARO, KAERI, the actual test was performed at the Korea Institute of Energy Research (KIER), Korea. Figure 3 shows the data collected for these operations. Since the performance of each case (before and after discharging test) is similar, it is thought that there is no serious change in the PEMFC.

2.2 Neutron Imaging Facility and System

All the experiments described above were performed at CONRAD, HMI. The CONRAD has two measurement positions(highest neutron flux and highest L/D ratio positions) with different neutron intensities (from 1×10^7 to 2×10^8 n/cm^{2}s) and L/D ratios (from 70 to 500). The neutron intensity is the highest at the front position towards the source, while the collimation ratio is the best at the position with the greatest distance from the source. Due to a poor spatial resolution at a highest neutron flux position, the test was performed at highest L/D ratio position. The neutron flux and L/D ratio for the current test are 1×10^7 n/cm^{2}s and 250, respectively.

The detecting system of this feasibility test consists of a neutron-sensitive scintillator and lens-CCD camera with a 16-bit (Andor DW436N-BV) with 2048 by 2048 pixels housed in a light tight box. The neutron beam is converted into light by the scintillator. The light is reflected by a mirror and then measured by the CCD camera. This design protects the camera against a neutron beam [14]. The beam size at the second position is approximately 10 $\times$ 10 cm^2. Although this lens-CCD camera system has a high spatial resolution, less than 100 μm, the system spatial resolution is limited to ~ 200 μm because of the scintillator. The temporal resolution is almost 15 seconds

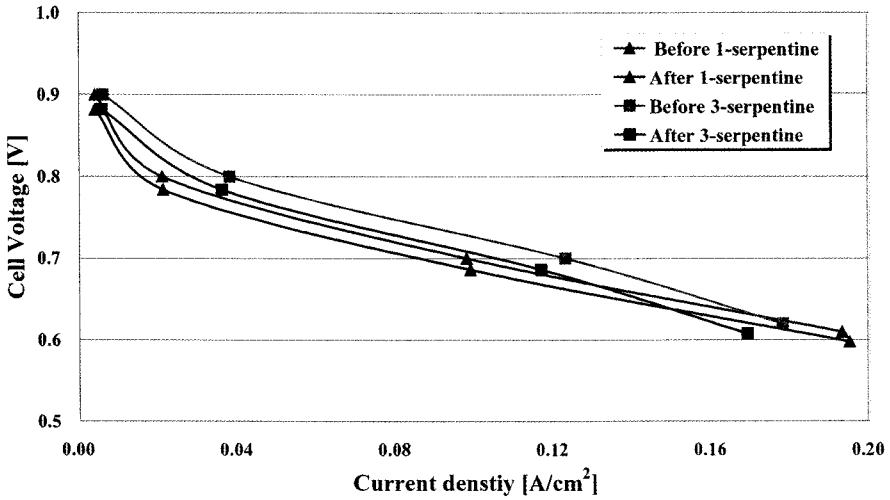

Fig. 3. Cell Polarization Curve

(exposure time is 10 seconds and data downloading time is about 5 seconds) due to low neutron flux.

2.3 Image Processing Procedure

The raw neutron image has the information for PEMFC as shown in Figure 4. The white area is an area of high neutron transmission, and the black area is one of low neutron transmission for the raw neutron image. Since neutrons are highly attenuated by water, the area of water is shown as a black region in the neutron image if water exists at PEMFC. Image processing is required in order to quantify the water content, although a raw neutron image can be used for a non-destructive test. Eq. (1) is the relationship between the neutron beam and attenuation due to the materials.

$$\Phi = \Phi_o \exp\left(-\sum_i \mu_i t_i\right) \tag{1}$$

where Φ is the neutron beam flux in front of the scintillator and Φ_o is the uninterrupted neutron beam flux upstream of PEMFC. The exponent accounts for an attenuating due to all materials, i, within the beam path; μ is the linear attenuation coefficient of the cold neutron; and t is the thickness of the element in the beam path. The linear attenuation coefficient is found by calibration or from the literature. The exponent contains a sum consisting of the μt products for all the materials. Division of an image of an operating fuel cell (***wet*** image) into an image of a non-operating fuel cell (***dry*** image) results in subtraction of the exponents and isolation of the change in water content. The detailed order of the image processing step is as follows [11, 12]:

(1) Capture images of the non-operating fuel cell (called ***dry*** image)
(2) Capture images of the operating fuel cell (called ***wet*** image)
(3) Dry and wet images are normalized by using the reference position as shown at Figure 4.
(4) Divide the ***wet*** image by the ***dry*** image and use a negative natural log to obtain the value of μt.

$$T = -\ln\left(\frac{\Phi_{wet}}{\Phi_{Dry}}\right) = -\ln\left[\frac{\Phi_o \exp\left(-\sum_i \mu_i t_i - \mu_{water} t_{water}\right)}{\Phi_o \exp\left(-\sum_i \mu_i t_i\right)}\right] = \mu_{water} t_{water} \tag{2}$$

(5) Finally the water thickness or volume can be calculated if the linear attenuation coefficient of water is known.

$$t_{water} = \frac{T}{\mu_{water}} \quad \text{or} \quad V = t_{water} \times A \tag{3}$$

Figure 5 shows a processed neutron image of a fuel cell as described by Eq.(2). The product μt is then obtained by computing the negative natural logarithm of each pixel fraction in Figure 5. Although the processed images in Figure 5 show variations in the liquid water content associated with variations in the gray scale, it is difficult to visualize small gradients because the maximum dynamic range of the values present in the gray scale images is set at 256 levels. Color scales exaggerate the image gradients to allow one to view a larger dynamic range of information. To create a color image from a gray scale image, the gray scale of the μt values from 0.1

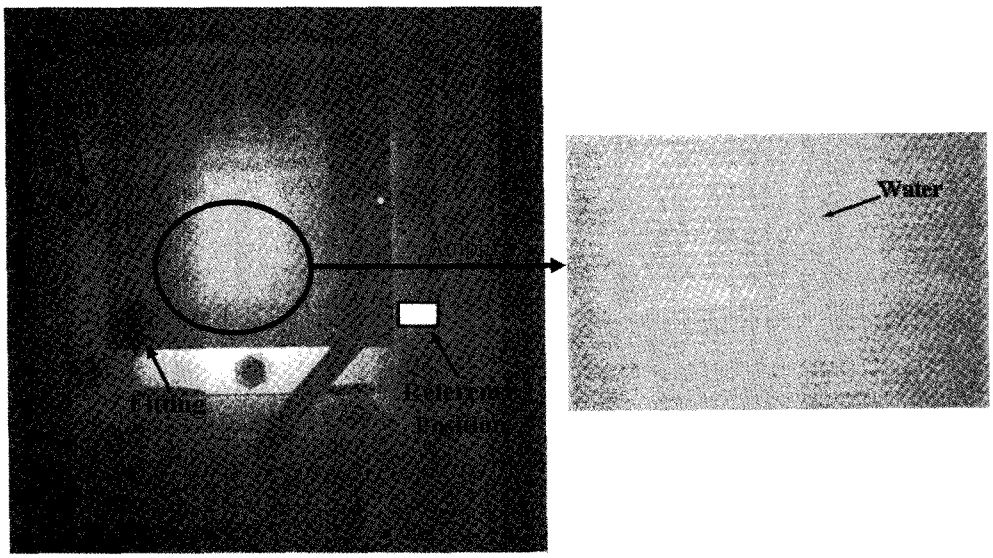

Fig. 4. Raw Wet Neutron Image with 10 Seconds at the Highest Neutron Flux Position

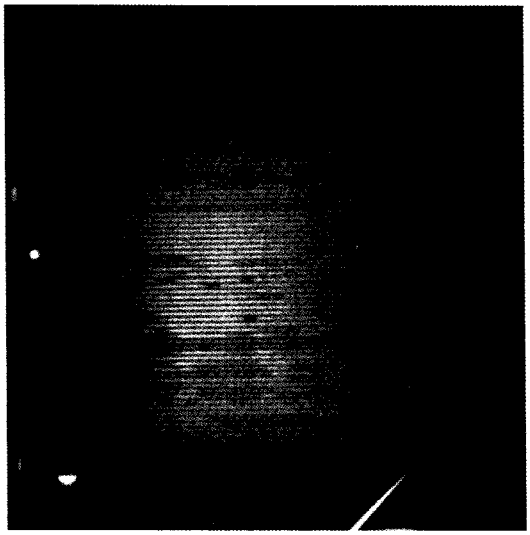

Fig. 5. Processed Wet Neutron Image by a Dry Neutron Image with 10 Seconds at the Highest L/D Ratio Position

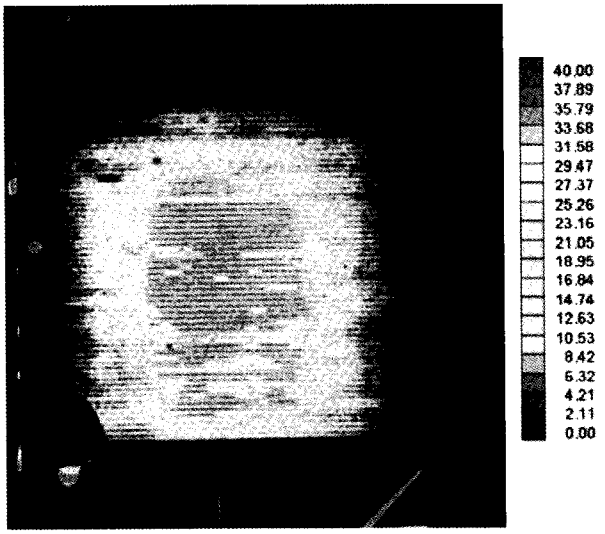

Fig. 6. Colorized Wet Image by Mapping the Gray Scale in Figure 5 to the RGB Scale

to 0.55 in Figure 6 was mapped to an RGB scale, as shown in Figure 5. The resulting image emphasizes the gradients in the liquid water thickness. Red means high water content; blue indicates less water content. By using these colorized neutron images, we made a neutron movie for each test condition. This neutron movie means that all neutron images were set in the sequence taken during test. Because of the flow direction of the cathode and anode, and the color density variation, we can easily discriminate the water behavior and position.

At steps (1) and (2) we must consider the white spots that are caused by gamma radiation hitting the CCD chip. For this purpose, a smoothing filter like a 3x3 median filter is applied to the whole data set. This technique consists of replacing the pixel value with the median of the neighboring pixel values.

2.4 Calibration of Linear Attenuation Coefficient

The linear attenuation coefficient of water must be known to calculate the water thickness. This linear attenuation coefficient usually depends on the neutron beam spectrum. The neutron beam is a Maxwellian

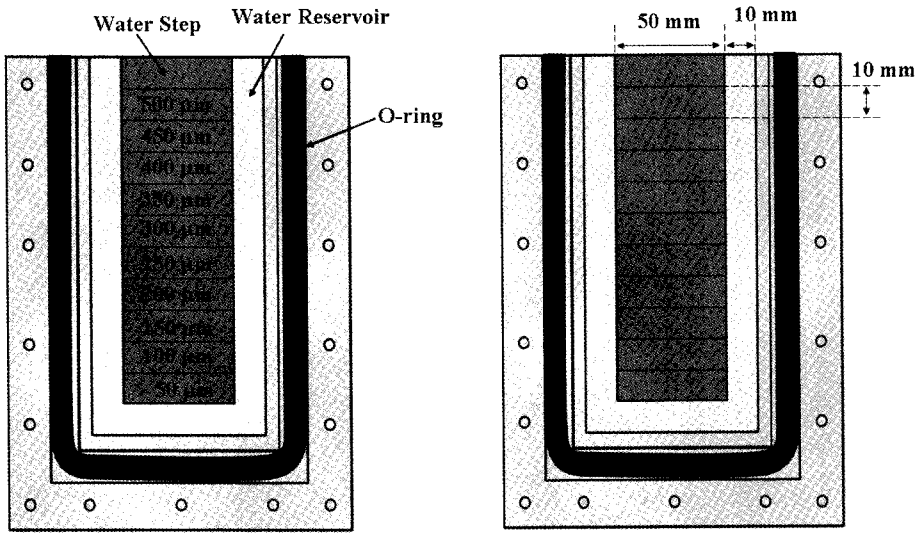

Fig. 7. Schematic Diagram of the Reference Specimen

distribution of neutrons and therefore the linear attenuation coefficient is averaged over many different neutron energies. To avoid an uncertainty of this value, the linear attenuation coefficient for water at the beam of the CONRAD was measured. Figure 7 shows the reference device constructed to allow for many thicknesses of the water. It consists of 10 steps of machining into an aluminum plate with each step 50 μm thicker than the previous step. Figure 8-a) is neutron image that was processed with dry and wet neutron images as described in Section 2.3. In order to eliminate the neutron flux variation effect, the reference position was arbitrarily selected outside the water step as shown in Figure 8-a). Because air was unexpectedly entrapped at some water steps, the data extraction positions didn't agree vertically. Since each water step has the same water thickness (the manufacturing tolerance is less than 5 μm), the position isn't a problem if the data were extracted at the same water step. Figure 8-b) shows the average gray level image versus the measured step thickness of the water. From the slope of a linear least squares fit of the data in Figure 8-b) the value of the linear attenuation coefficient is determined to be 0.597±0.004 mm^{-1}. This is almost twice that of the value for thermal neutrons. This shows that the cold neutron is more sensitive than the thermal neutron for water detection at PEMFC.

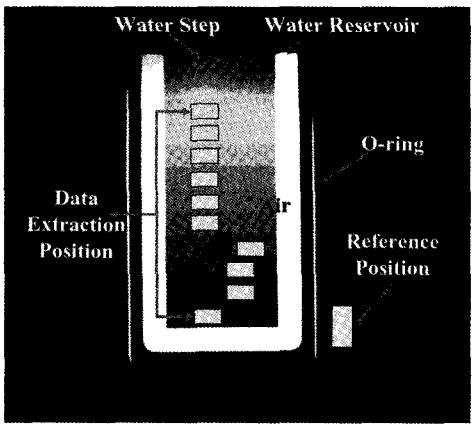

(a)

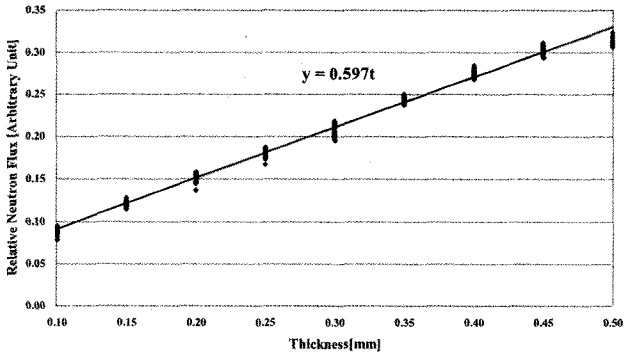

(b)

Fig. 8. Calibration of the Linear Attenuation Coefficient for Water: (a) Neutron Image and (b) Calibration Curve

3. RESULTS AND DISCUSSION

A feasibility test was performed in order to investigate the water discharge characteristics for different flow field types and flow rates. In this feasibility test, the two geometries sketched in Figure 2 were used; 1-parallel serpentine and 3-parallel serpentine types. Based on checking the water level at the outlet of the cathode side by naked eye, most of the water was discharged as soon as the pressurized air was supplied. Although the discharging time of the water at the cathode depends on the flow rate, it was difficult to discriminate the discharging characteristics of the water due to the relatively long exposure time (10 seconds).

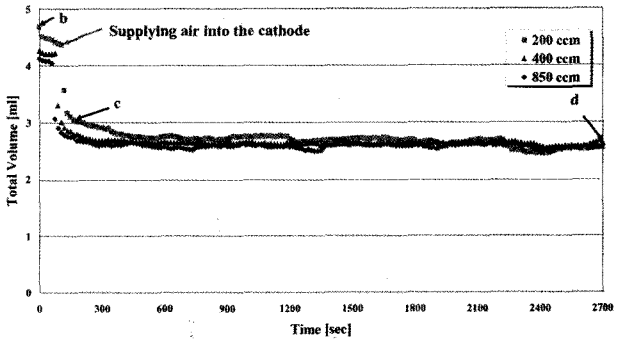

(a)

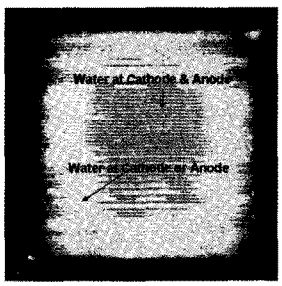

(b)

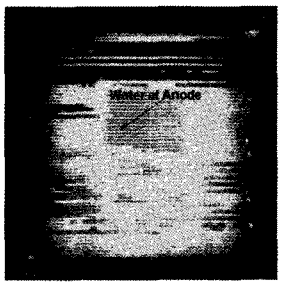

(c)

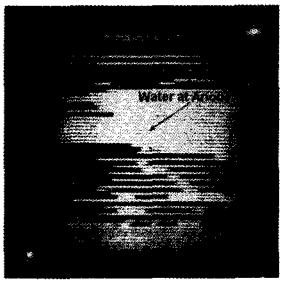

(d)

Fig. 9. (a) Total Water Volume Variation and Neutron Images of (b) Before Start, (c) after 120 Seconds, (d) after 3000 Seconds at 1-Channel Serpentine with 200 cc/min

Figure 9 shows the test results of the water discharge characteristics for the 1-parellel serpentine type under different flow rates. Total water volume is calculated as described in Section 2.3. After supplying pressurized air regardless of the flow rate, the total water volume is sharply decreased as shown at Figure 9-a). These results come from the removal of water at the cathode channel. However, the total water volume is almost constant after discharging the water at the cathode channel because the water at the anode side wasn't discharged. These results were confirmed by visualization results using the neutron imaging technique as shown in Figures 9-b), 9-c), and 9-d).

Figures 9-b) to d) are the colorized neutron images; one is before supplying pressurized air, the second is after 120 seconds, and the other is after 2700 seconds. The red color in every figure means a high water fraction and the black color stands for a low water fraction. Since water was only supplied to the cathode side, it was thought that the water was only at the cathode side. However, there was awater movement from the cathode to the anode side when investigating the neutron images. This result comes from diffusion phenomena due to a difference of the water fraction between the cathode and the anode. In the present test, the existence of water at the anode was confirmed by a movie made from the neutron images. When comparing Figures 9-b) and 9-c), there is a color change due to the removal of the water at the cathode channel. Therefore the red color in Figure 9-b) indicates that water exists at the cathode and anode sides. The yellow area means water only exists at the cathode or anode side in Figure 9-c). Because a neutron image is a line integral of beam direction, it is difficult to discriminate the position of water, except when using 3-D tomography. The water at the anode side still remains, as shown in Figure 9-d), because of the lack of supply of pressurized air into the anode side. (Since the test results of the other conditions were similar, those visualization results weren't displayed.)

Figure 10 shows the test results of the water discharge characteristics for the 3-parellel serpentine type under different flow rates. Test results are similar to those of 1-parallel serpentine type except for the value of 850 cc/min. Although the total water volume of the 400 cc/min case after supplying pressurized air is higher than that of the 200 cc/min case, as shown at Figure 10-a), this isn't related to efficiency of flow rate. Because we can't control the initial water level, especially the water level of the anode side, these problems occur. Total water volume of in the 200 and 400 cc/min cases is almost constant because water at the anode side wasn't removed.

On the other hand, the 850 cc/min case is different. When supplying pressurized air into the cathode channel, the water at the cathode channel is discharged, as shown in Figures 10-a) and 9-c). However, water at the anode side is also monotonically removed and finally most of the water at the cathode and anode side was removed after 1500 seconds for the 850 cc/min case, as shown in Figure 10-d). This means that there was a momentum force from the cathode to the anode when compared with the other conditions. Most of the water at the anode channel was removed due to this force. Detailed research for these phenomena will be needed. However, it is difficult to remove water from the bottom of the fuel cell since the channel isn't optimized to completely discharge the water. Moreover, a white area in Figure 10-d) means that water doesn't exist in the channel, but only at the MEA. This result shows the merit of the neutron imaging technique when compared with the other methods. Though the visualization method with a transparent window can discriminate water movement and distribution in a channel of the PEMFC, it is impossible to see the MEA of the PEMFC.

Since an auto-vehicle can run in sub-zero temperature conditions, the freezing of water at the MEA causes

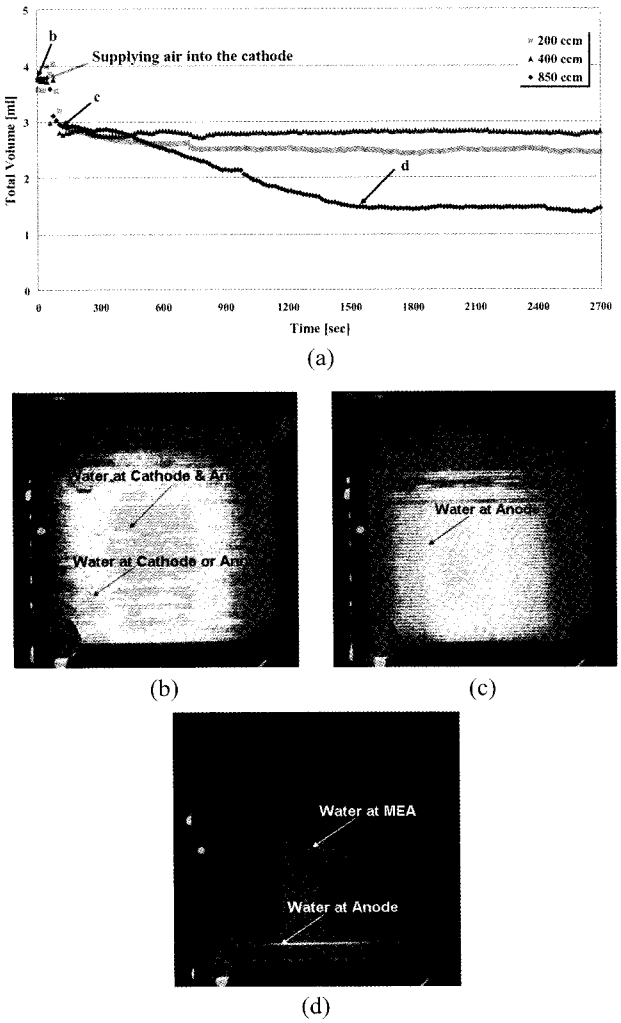

Fig. 10. (a) Total Water Volume Variation and Neutron Images of (b) Before Start, (c) after 90 Seconds, (d) after 1500 Seconds at 3-Channel Serpentine with 850 cc/min

damage to the MEA. Therefore, water at the PEMFC, regardless of its position, must be removed as soon as possible. Thus, the water was not removed by using the pressurized air method during these feasibility tests, regardless of the flow field geometries and flow rates. In order to remove water at PEMFC, a special treatment is needed at the PEMFC; for example using heating, a micro-channel for the removal of water, and so on. The neutron imaging technique is a powerful tool to improve the water removal efficiency at the PEMFC.

4. CONCLUSIONS

A series of measurements has been conducted to investigate the water discharge characteristics by using cold neutrons and a feasibility test apparatus at CONRAD, HMI. Although it was difficult to analyze the transient phenomena of water movement and distribution in PEMFC because of the long exposure time, it will be helpful to improve the efficiency of PEMFC since the neutron imaging technique had the ability to visualize not only the channels but also the MEA. There is water movement from the cathode to anode side that is visible when comparing the neutron images. Water at the cathode channel is well removed by pressured air. Except for the 3-parellel serpentine with 850cc/min case, most of the test results are similar. During the feasibility tests, water at the MEA isn't removed under any conditions. Therefore, special treatment for water removal is required.

ACKNOWLEDGMENTS

This study was supported by the Korea Foundation for International Cooperation of Science and Technology (KICOS) through a grant provided by the Korean Ministry of Science & Technology (MOST) in M60602000005-06E0200-00410.

NOMENCLATURE

A	area (mm^2)
D	collimator aperture
GDL	Gas Diffusion Layer
L	Distance from a collimator to scintillator
L/D ratio	Main factor to define a spatial resolution of neutron imaging technique (also called collimation ratio)
MEA	Membrane Electrode Assembly
PEMFC	Polymer Electrolyte Membrane Fuel Cell
t	Thickness (mm)
T	Relative neutron flux ratio
Φ	Neutron flux of front of scintillator (n/cm^2s)
Φ_0	Uninterrupted neutron beam flux (n/cm^2s)
μ	Linear attenuation coefficient (mm^{-1})

Subscripts

dry	Without water
wet	With water

REFERENCES

[1] W. Vielstich, A. Lamm, and H. Gastiger, *Handbook of Fuel Cells – Fundamentals, Technology, Application*, New York: Wiley, 2003.
[2] R.J. Bellow, M.Y. Lim, M. Arif, A.K. Thompson, and D. Jacobson, J. Electrochem. Soc., 146, 1099, (1999).
[3] R. Satija, D.L. Jacobson, M. Arif, and S.A. Werner, J. Power Sources, 129, 238, (2004).
[4] Kramer, D., and E. Lehmann, Nuclear Instruments and Methods in Physics Research, Section A: Accelerators, Spectrometers, Detectors and Associated Equipment, 542(1-3), 52-60, (2005).
[5] Kramer, D., and J. Zhang, Electrochimica Acta, 50(13), 2603-2614, (2005)
[6] Pekula, N., and K. Heller, Nuclear Instruments and Methods in Physics Research, Section A: Accelerators, Spectrometers, Detectors and Associated Equipment, 542(1-3), 134-141, (2005)
[7] Schneider, I.A. and D. Kramer, Electrochemistry Communications, 7(12), 1393-1397, (2005)
[8] Zhang, J., and d. Kramer, Electrochimica Acta, 51(13), 2715-2727, (2006)
[9] Hickner, M.A. and N.P. Siegel, Journal of the Electrochemical Society, 153(5), (2006)
[10] A. Hilgera, N. Kardjilov, M. Strobla, W. Treimera, and J. Banhart, Physica B, 385–386, 1213–1215, (2006).
[11] D.J. Ludlowa, C.M. Calebrese, S.H. Yu, C.S. Dannehy, D.L. Jacobson, D.S. Hussey, M. Arif, M.K. Jensen, G.A. Eisman, J. Power Sources, 162, 271-278, (2006)
[12] TaeJoo Kim, CheulMuu Sim, and MooHwan Kim, Applied Radiation and Isotopes, (In printing)
[13] K. Tuber, D. Pocza, and C. Hebling, J. Power Sources, 124, 403-414, (2003).
[14] A. Hilgera, N. Kardjilov, M. Strobla, W. Treimera, and J. Banhart, Physica B, 385–386, 1213–1215, (2006)